Improved Design and Analysis of Self-Powered Synchronized Switch Interface Circuit for Piezoelectric Energy Harvesting Systems

Junrui Liang, *Member, IEEE*, and Wei-Hsin Liao, *Senior Member, IEEE*

***Abstract*—In piezoelectric energy harvesting (PEH), with the use of the technique named synchronized switch harvesting on inductor (SSHI), the harvesting efficiency can be greatly enhanced. Furthermore, the introduction of its self-powered feature makes this technique more applicable for stand-alone systems. In this paper, a modified circuit and an improved analysis for the self-powered SSHI (SP-SSHI) are proposed. With the modified circuit, direct peak detection and better isolation among different units within the circuit are achieved, both of which result in the further removal on the dissipative components. In the improved analysis, details in the open circuit voltage, switching phase lag, and intermediate voltages among different phases are discussed, all of which lead to a better understanding on the working principle of SP-SSHI. The total power dissipation from the piezoelectric source is also investigated. It is of concern but has not been considered in the previous literatures. Both analyses and experiments show that, in terms of the harvested power, the higher the excitation level, the closer between SP-SSHI and ideal (externally powered) SSHI; at the same time, the more beneficial the adoption of SP-SSHI treatment in PEH, compared to the standard energy harvesting (SEH) technique. Under the four excitation levels investigated, the SP-SSHI can harvest up to 200% more power than the SEH interface circuit.**

***Index Terms*—Energy flow, energy harvesting, interface circuit, piezoelectric, self-powered.**

I. Introduction

STRUCTURED by a certain number of spatially distributed autonomous sensor devices, the wireless sensor networks (WSNs) can be used in military, industrial, and civil applications for monitoring different physical and environmental conditions [1]. Many concerns on energy consumption were addressed due to their nature on wireless connections [2]. Different energy harvesting techniques have been investigated for the purpose to broaden the energy sources, alleviate the dependence on batteries, and hopefully someday make all WSN devices self-powered [3]–[6].

Manuscript received January 29, 2011; revised June 24, 2011; accepted August 15, 2011. Date of publication September 6, 2011; date of current version November 1, 2011. This work was supported by the Research Grants Council of the Hong Kong Special Administrative Region, China under Project CUHK 414809.

The authors are with the Department of Mechanical and Automation Engineering, The Chinese University of Hong Kong, Shatin, Hong Kong (e-mail: jrliang@mae.cuhk.edu.hk; whliao@cuhk.edu.hk).

Color versions of one or more of the figures in this paper are available online at http://ieeexplore.ieee.org.

Digital Object Identifier 10.1109/TIE.2011.2167116

Piezoelectric energy harvesting (PEH) is one of the promising techniques that can scavenge energy from the ambient vibration sources [4], [7]. With its electromechanical coupling characteristic, a piezoelectric element can generate electricity when strain is produced. Since the deformation in a vibrating structure is alternating, the generated electricity is also alternating. On the other hand, the most potential applications for the PEH techniques are WSNs and portable electronics [3]. In these electronic devices, dc power supply is required. Moreover, the storage of electrical energy also requires electrical energy in dc form. Therefore, an interface circuit is needed for ac-dc conversion. The standard energy harvesting (SEH) interface circuit involves only a bridge rectifier for the ac-dc conversion [8]–[10]. The energy harvesting capability can be enhanced by adopting different kinds of switch interface circuits [11]–[13]. In particular, Guyomar *et al.* proposed a nonlinear technique named synchronized switch harvesting on inductor (SSHI) [14]. It was claimed that, under the same displacement excitation, SSHI can increase the harvested power by several hundred percent, compared to SEH [11], [14]–[16]. The improvement would be more significant for weakly coupled PEH systems [17], [18]. To implement SSHI, a displacement sensor and a controller were usually needed for synchronization and generation of the switching commands [11], [14], [19], [20]. The power consumption of these auxiliary devices could be even higher than the harvestable power [21]. Two solutions can be adopted for implementing SSHI in practical PEH systems. The first is to cut down the power consumption of the auxiliary units (usually integrating them into an integrated circuit), until it could be covered by the harvested power [22]. The second is to build a self-powered SSHI (SP-SSHI) interface circuit, which can automatically switch at voltage peaks without regulated power supply [21], [23]–[25]. In SP-SSHI, the synchronization is carried out based on the information from the peak detectors; at the same time, the switches, which are in fact powered by the piezoelectric source, automatically take actions to invert the piezoelectric voltage once the maxima or minima are attained.

Lallart and Guyomar [21] implemented the SP-SSHI interface circuit with some discrete electrical components. Based on the experiment, they claimed that their SP-SSHI interface circuit can harvest 1.6 times more power than the SEH one. They have also considered the influence of the voltage drops, which are produced by diodes and transistors in the circuit, over the harvested power. Yet, the influences of other components, such as the capacitors in the envelope detectors, have

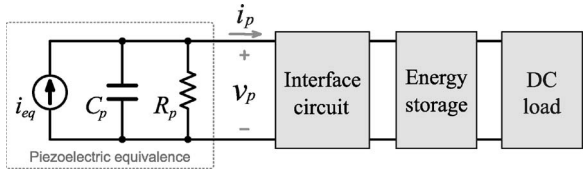

Fig. 1. Equivalent circuit of a PEH device.

not been pointed out. In addition, two important parameters, i.e., the switching delay phase φ and inversion factor γ, were regarded as constants. However, in fact, these two parameters are constants only when the open circuit voltage V_{OC} (related to displacement magnitude) and storage voltage V_{DC} (voltage across the storage device) are constants. A more complete analysis should take these into account, for comparing the energy harvesting efficiencies under different V_{OC} and V_{DC}. Instead of using transistors to switch the inductor shunt, Qiu *et al.* [24] used two silicon controlled rectifiers to construct their SP-SSHI interface circuit; yet, analysis on the principle and performance details about the proposed circuit was lacked.

In the aforementioned literatures, the energy dissipation in the SP-SSHI circuit and the performance difference between the SP-SSHI and ideal (externally powered) SSHI interface circuits were not shown. Without considering these issues, the cost for implementing the self-powered switching actions cannot be specified. Moreover, in either literature, only the performance of the SP-SSHI device under a specified vibration magnitude was investigated. Given that, in SP-SSHI, a part of the harvested power must be consumed to carry out the switching actions, it would be too strong to conclude that SP-SSHI always outperforms SEH.

In this paper, a modified circuit topology for SP-SSHI is proposed. The circuit is built with discrete electrical components. With the adoption of a complementary topology, the peak detection units can be separated from the switching inductive shunt; therefore, better isolation can be achieved. An improved analysis is also provided considering the aforementioned concerns about SP-SSHI. Section II introduces the working principles of PEH as well as the SSHI interface circuit. Section III proposes the modified circuit topology for SP-SSHI. Section IV provides an improved analysis on SP-SSHI. Section V compares and discusses the experimental and analytical results. Section VI concludes the paper.

II. Principles

A. Piezoelectric Energy Harvesting

Given a typical PEH device, e.g., a piezoelectric cantilever with harvesting interface circuit and energy storage, the piezoelectric structure can be modeled as an equivalent current source i_{eq} in parallel with the piezoelectric clamped capacitance C_p and the internal leakage resistance R_p, as shown in Fig. 1. The current source i_{eq} is proportional to the vibration velocity $\dot{x}$ with the relation of

$$i_{eq}(t) = \alpha_e \dot{x}(t) \tag{1}$$

where α_e is the force-voltage factor of the piezoelectric structure.

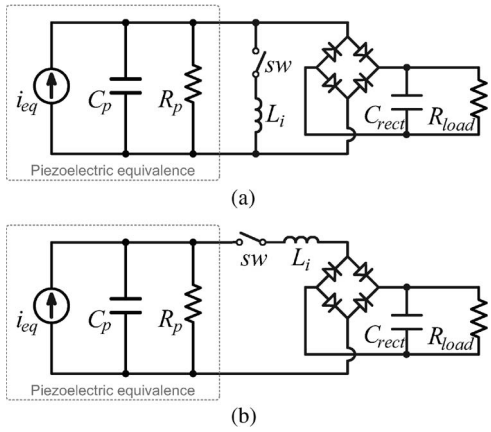

Fig. 2. Equivalent circuits of two SSHI treatments. (a) P-SSHI. (b) S-SSHI.

Different interface circuits could be designed for different objectives; yet, in terms of energy flow, they all extract energy from the vibrating mechanical structure. For the purpose of vibration suppression, usually the extracted energy is dissipated, while for energy harvesting, a portion of the extracted energy is reclaimed and stored in electrical form for the subsequent usage. As shown in Fig. 1, for a PEH device, the interface circuit provides power conditioning, and then the energy storage device stores the harvested energy, while a part of the harvested energy is used to power the dc load.

B. SSHI Interface Circuit

In a vibrating piezoelectric device, since the induced voltage across the piezoelectric capacitance is alternating, the most conventional way to turn an ac voltage into dc is to use a bridge rectifier for rectification and then a capacitor for filtering. The combination of bridge rectifier and filter capacitor forms the standard interface circuit that can be used for energy harvesting, i.e., SEH. Ottman *et al.* [8], [9] discussed the optimization of the SEH technique. Yet, using SEH cannot ensure that the energy is always flowing from the mechanical part to the electrical part. During a certain interval in each cycle, energy returns from the electrical part to the mechanical part. It was called the *energy return phenomenon* [16].

The SSHI treatment overcomes this problem by adding an inductive switch path, which is composed of a switching component sw and an inductor L_i to the SEH circuit. This path can be connected in parallel to the bridge rectifier to form a parallel SSHI (P-SSHI) circuit [Fig. 2(a)], or in series to form a series SSHI (S-SSHI) circuit [Fig. 2(b)] [11]. Regardless of P-SSHI or S-SSHI, the switch switches on to form the series loop once the displacement x reaches its extreme values, and then switches off after half of an resistance inductance capacitance (RLC) cycle, as shown in Fig. 3(c), so as to allow a natural inversion to v_p, the voltage across the piezoelectric element. Since the period of the RLC circuit $2\pi\sqrt{L_i C_p}$ is usually selected to be much smaller than the vibration period that equals to $2\pi/\omega$, the voltage inversion is regarded to be finished in an instant. On the other hand, the vibration period is much smaller than the time constant $R_p C_p$, the influence of R_p during the switching-on interval is negligible.

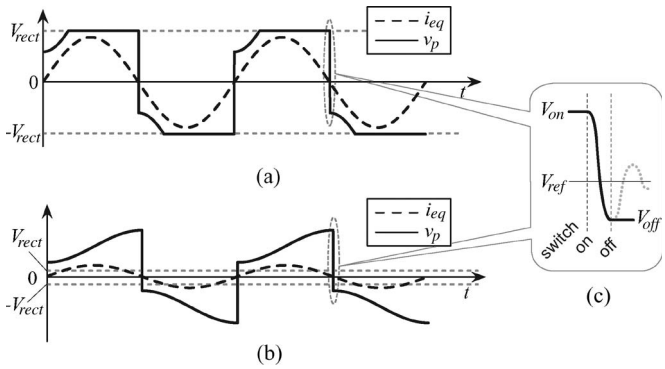

Fig. 3. Typical waveforms of two SSHI treatments. (a) P-SSHI. (b) S-SSHI. (c) Inversion of v_p at the instant of extreme displacements.

The voltage relation before and after the switching action in SSHI is described by the following equation:

$$V_{off} - V_{ref} = \gamma(V_{on} - V_{ref}) \tag{2}$$

where V_{on} and V_{off} are the voltages before and after the inversion, respectively; V_{ref} is the reference voltage; γ is the inversion factor that is defined as[1]

$$\gamma = -e^{-\pi/(2Q)}. \tag{3}$$

Q is the quality factor of the $sw - L_i - C_p$ loop. In P-SSHI, V_{ref} equals to zero; in S-SSHI, V_{ref} equals to the rectified voltage V_{rect}, which is the sum of the voltage drop of a practical rectifier and the storage voltage V_{DC}, i.e., the voltage across the filter capacitance C_{rect}.[2] Typical waveforms in P-SSHI and S-SSHI as well as the zoom-in view of one of their switching intervals are shown in Fig. 3. Since i_{eq} is proportional to the velocity $\dot{x}$, these switching actions make sure that v_p and i_{eq} have the same sign; therefore, their product, the power input from the mechanical part to the electrical part, is always positive.

To implement SSHI, additional units for displacement peak detection and switch control are required. In most of the researches, these functions were realized with displacement sensors and digital controllers [11], [14], [19], all of which need external power to run. In [21], all these units were replaced by an SP-SSHI circuit.[3] It makes use of the piezoelectric element itself as a displacement sensor and generates switching commands with transistors accordingly. The introduction of this SP-SSHI allows the SSHI technique to be more compact and independent of the external power and therefore opens a more promising future to the SSHI technique. Yet, some concerns about the SP-SSHI were still not addressed in [21]. For example, is there any constraint or applicable range for this treatment? Does the SP-SSHI always outperform SEH? In the following sections, the SP-SSHI treatment will be further investigated concerning these issues.

III. Circuit

The essence of the SP-SSHI technique proposed in [21], [23], [24] is the electronic breaker. Without providing external power, it can automatically perform switching actions once the voltage across the switch reaches its maxima. Since one breaker can only allow the current flow in one direction, replacing the switch in either Fig. 2(a) and (b) with two of such breakers (one as maximum breaker and the other, which was inversely connected, as minimum breaker), the SP-SSHI can be achieved. The breaker consists of three parts: envelope detector, comparator, and switch. In the design presented by Lallart and Guyomar [21], the envelope detectors were in series with the clamped capacitance C_p and inductor L_i. The detected voltage in fact was not v_p, but the voltage sum of v_p and the voltage across L_i. Even L_i is connected to C_p for a very short interval in every cycle, the hard switching-off action introduces high frequency components to L_i. The local maxima or minima produced by these high frequency components may induce misjudgment to the other breaker. Therefore, both the envelope detector and comparator parts should be carefully isolated from the switching path. For the breaker introduced in [21], [24], several resistors were connected for the isolation purpose. Yet, the principle and design guideline were not clearly provided.

Taking these envelope detection and isolation issues into consideration, in our self-powered design, we use complementary transistors topology to achieve both direct envelope detection for v_p and reduction on the interference among different parts in the breakers. With this reformation, all the isolating resistors, which are bound to consume some energy, can be removed. The modified SP-SSHI circuit for S-SSHI is shown in Fig. 4.[4] We obtain its waveforms (Fig. 5), as well as the zoom-in view around one of the processes of switching on maxima (Fig. 6) with the PSpice simulation. The component values and models used in simulation are listed in Table I. v_{C1} and v_{C2} in Fig. 5 denote the voltages across C_1 and C_2; i_{D5}, i_{D6}, i_{C1}, and i_{C2} in Fig. 6 denote the currents flowing through D_5, D_6, C_1, and C_2, respectively.

Accompanying with the vibration, switching actions take place when v_p reaches its maximum or minimum in each cycle. Different from the ordinary SSHI interface, which has only one voltage inversion in each switching action, in the SP-SSHI circuit, two voltage inversions and one charge neutralization are experienced accompanying with each switching action, which can be figured out from the voltage and current waveforms within the switching intervals, as shown in Fig. 6. Combining with the natural charging phase toward maximum or minimum, we can divide half of a vibration cycle into four phases.

Take the half vibration cycle associated with switching on maximum for discussion. Fig. 7 shows the detailed working principle of the four phases. For the switching on maximum, R_1, D_1, and C_1 form an envelope detector. T_1 acts as a comparator while T_3 acts as the electronic switch.

[1]The definition on voltage inversion factor in this paper is different from that in [21]. The sign information is also included in this definition.

[2]Since C_{rect} is usually selected to be much larger than C_p, V_{DC} is regarded constant during each vibration cycle.

[3]More exactly, it is a self-powered S-SSHI device in [21].

[4]The self-powered interface circuit for P-SSHI can be modified from that for S-SSHI. In this paper, the analysis and experiment focus on the S-SSHI case for showing the principle and insights about the self-powered switching interface circuit.

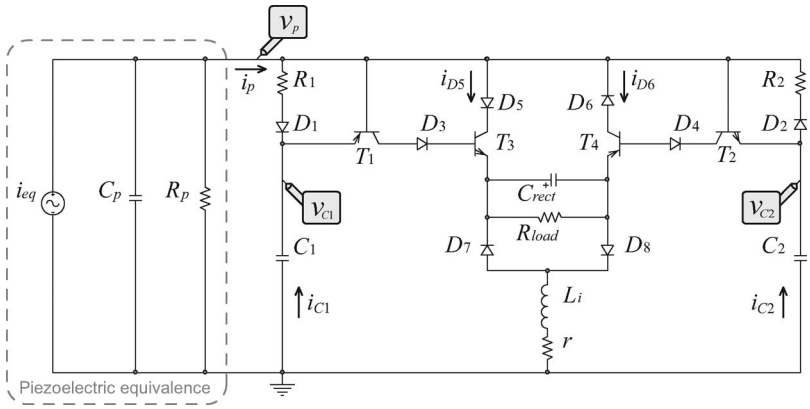

Fig. 4. Modified SP-SSHI interface circuit.

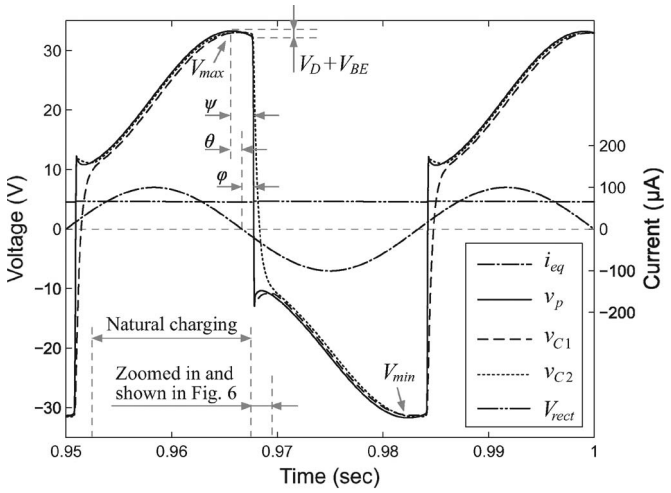

Fig. 5. Simulation waveforms in the modified SP-SSHI.

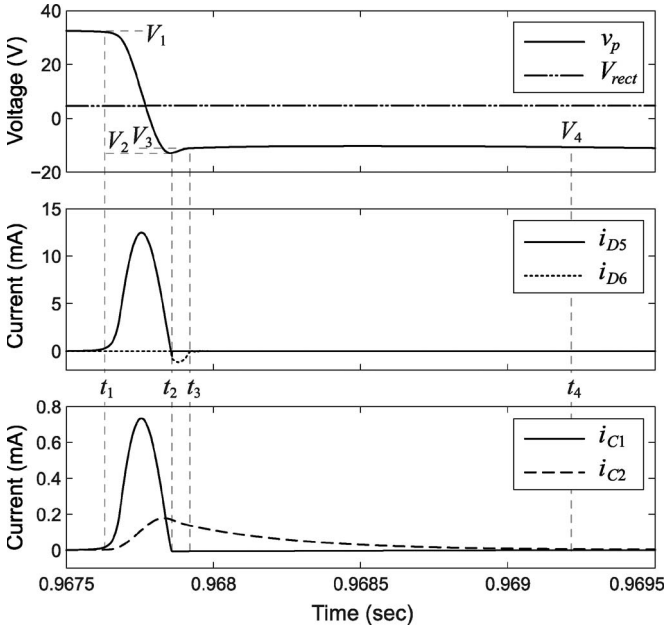

Fig. 6. Voltage and current waveforms in the process of switching on maximum.

Natural Charging: The current flow in the phase of natural charging toward the maximum value of v_p is shown in Fig. 7(a). In this phase, only the paths of the two envelop detectors in the interface circuit conduct; all transistors are cut off. Positive equivalent current i_{eq} charges C_p, C_1, and C_2, so that v_p, v_{C1}, and v_{C2} increase simultaneously, as shown in Fig. 5.

TABLE I
COMPONENT MODELS OR VALUES

Component	Model / value
C_p	33.74 nF
R_p	2.08 MΩ
R_{ed} (R_1 and R_2)	200 kΩ
C_{ed} (C_1 and C_2)	680 pF *
Diodes (D_1 to D_8)	1N4004
PNP transistors (T_1 and T_4)	TIP32C
NPN transistors (T_2 and T_3)	TIP31C
C_{rect}	10 μF
L_i	47 mH
r	178.8 Ω

* C_{ed} is 2 nF in simulation for properly starting up the switching processes.

First Inversion: When v_p reaches its maximum V_{max}, the voltage across C_1 is $V_{max} - V_D$, where V_D denotes the forward voltage drop of a diode. Then, v_p begins to drop. When the decrease reaches $V_D + V_{BE}$,[5] i.e., $v_p = V_1$ (t_1 instant in Fig. 6), the transistor T_1 conducts. C_1 begins to discharge through $T_{1(ec)}$, D_3, $T_{3(be)}$, C_{rect}, D_8, L_i, and r (as observed from the i_{C1} waveform in Fig. 6), consequently makes T_3 conduct.[6] The conduction of T_3 switches on the inductive path that consists of D_5, $T_{3(ce)}$, C_{rect}, D_8, L_i, and r, producing a shortcut to the charge in C_p. C_p starts a quick discharge from the voltage V_1 through the inductive path (as observed from the i_{D5} waveform in Fig. 6), until v_p reaches its local minimum (t_2 instant in Fig. 6). The current flow in the first inversion is shown in Fig. 7(b).

Second Inversion: The current through L_i now tends to reverse its flowing direction, but the $T_{3(ce)}$ path is immediately blocked by the reverse D_5. As observed from Fig. 6, i_{D5} maintains at zero after the t_2 instant. Yet, the path consisting of D_7, C_{rect}, $T_{4(ce)}$, and D_6 is still available. Because even T_4 is cut off, there is a small parasitic capacitance across its emitter and collector, which is uncharged. The reverse current flows through this path, as it can be observed from the i_{D6}

[5] V_{BE} denotes the transistor base-emitter threshold voltage.

[6] The component r in Fig. 4 represents the total equivalent series resistance of the non-ideal switching path. It is composed of the parasitic resistances of the inductor, diodes, and transistors.

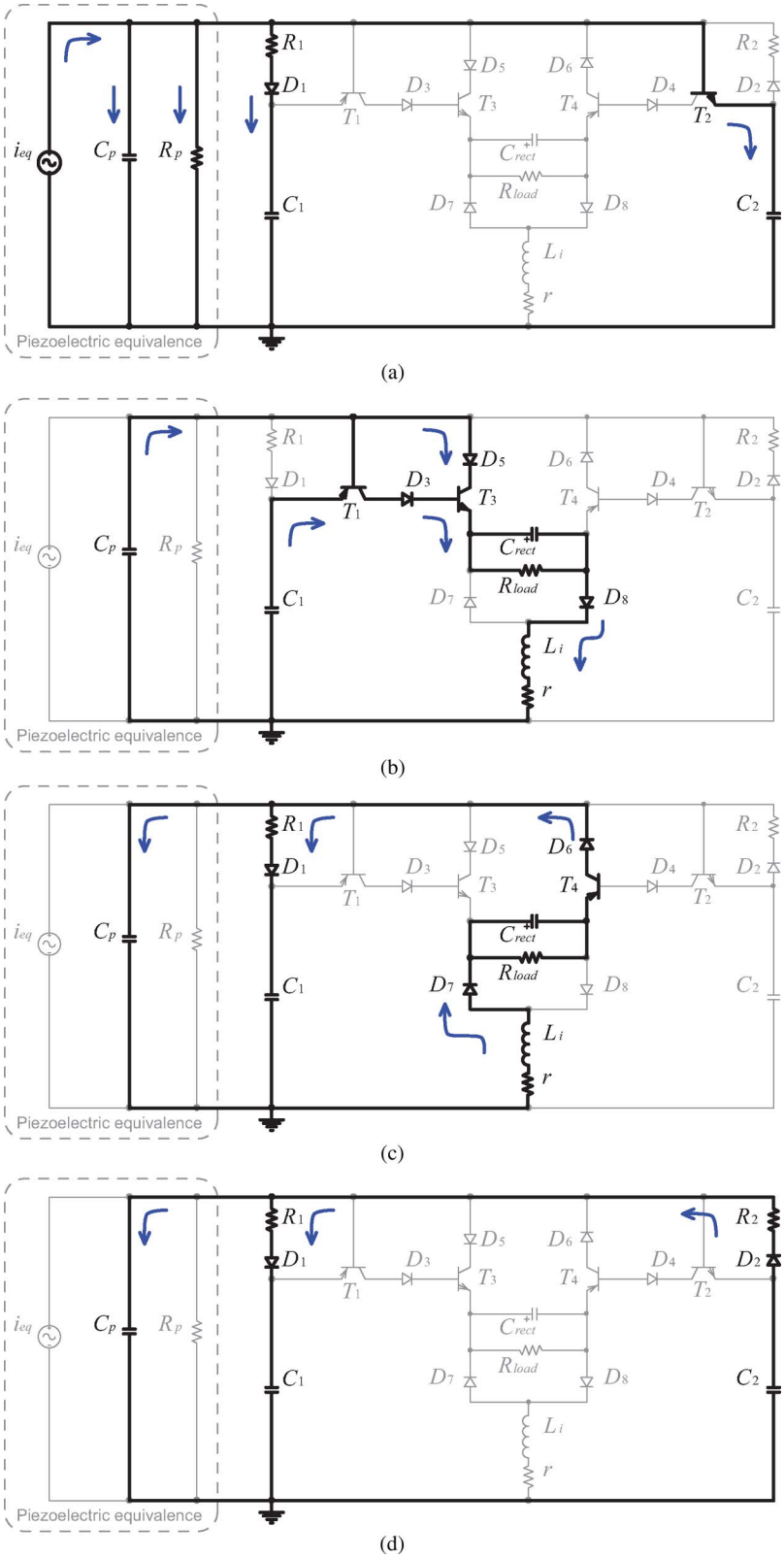

Fig. 7. Four phases within half of a vibration cycle (associated with switching on maximum). (a) Natural charging. (b) First inversion. (c) Second inversion. (d) Charge neutralization.

waveform in Fig. 6, until T_4's emitter-collector capacitance C_{CE} is charged, at which very instant (t_3 instant in Fig. 6) v_p becomes V_3. The local minimum of v_p, i.e., V_2, may induce misjudgment for the minimum breaker. Hence, R_2 is necessary for making sure that C_2, which is used for minimum detection, discharges slower than C_p, so as to skip over this local minimum. Fig. 7(c) shows the current flow in the second inversion. The second inversion is a side-effect in the self-powered

interface to counteract the energy conversion enhancement. This side-effect can be limited by selecting transistors with small emitter-collector capacitor capacitance C_{CE} as the switches. However, it cannot be completely got rid of, since the parasitic capacitance C_{CE} cannot be totally removed from a practical transistor.

Charge Neutralization: After t_3, both T_3 and T_4 are cut off; however, C_2 still has not finished its discharging, the rest of the charge in C_2 will flow into C_p and C_1 until they are the same in voltage. The discharge of C_2 is reflected by the i_{C2} waveform shown in Fig. 6. It stops when i_{C2} approaches zero (t_4 instant in Fig. 6). This charge neutralization again increases v_p a little bit to V_4 before v_p enters the following half cycle of minimum detection. The actual discharge of C_2 starts from t_1, as observed from the i_{C2} waveform in Fig. 6; yet, to simplify the analysis, the charge neutralization is assumed to be an independent phase other than the other three phases. The current flow in this charge neutralization phase is shown in Fig. 7(d).

Switching on minimum makes use of the counterparts in the circuit, and its principle is similar to that of switching on maximum. Because of the complementary topology, for the switching on minimum, the four intermediate voltages are $-V_1$, $-V_2$, $-V_3$, and $-V_4$, respectively. The analysis on the four phases within half of a vibration cycle helps understand the working principle of the SP-SSHI interface circuit and also provides guidance for the component selection. From the voltage waveforms of v_p, v_{C1}, and v_{C2} shown in Fig. 5, C_1 and C_2 in the envelop detectors are approximately connected in parallel to C_p. They affect the original system and decrease the magnitude of the open circuit voltage. This influence can be reduced by selecting small C_1 and C_2; yet, they cannot be too small, because the stored charge in these two capacitors should be enough to drive the corresponding transistors for carrying out switching actions. To determine the values of these two capacitors, some trial-and-error experiments should be involved, and the value might be different according to the selected transistors. On the other hand, the values of C_1 and R_1 (or C_2 and R_2, respectively) should satisfy the following criterion:

$$2\pi\sqrt{L_i C_p} < R_{ed}C_{ed} \ll \frac{\pi}{\omega} \tag{4}$$

where ω is the frequency of the mechanical vibration. Because the capacitors C_1 and C_2 in the envelope detectors are selected to be the same value, they are denoted as C_{ed} in (4); similarly, R_1 and R_2 are denoted as R_{ed}. The first inequality ensures that the charge neutralization finishes later than the two voltage inversions, so as to avoid the misjudgment on local minima or maxima. The second inequality implies that the charge neutralization should use much less time than half of a vibration cycle, so that the influence induced by inserting envelop detectors can be minimized.

IV. Analysis

In Section III, the working principle of the modified SP-SSHI circuit has been introduced. Based on this, detailed and quantitative analysis is provided in this section.

A. Open Circuit Voltage

The effect of the two capacitors C_1 and C_2 in the envelop detectors was not taken into account in [21]. Within one vibration cycle, the energy that is flowed into these two capacitors will return to the mechanical part rather than being stored in themselves nor used to power the dc load. Therefore, C_1 and C_2 can be equivalently regarded as two capacitors connected in parallel to C_p. This approximation is validated from Fig. 5, since both v_{C1} and v_{C2} are very close to v_p. Given the harmonic displacement excitation as

$$x(t) = X\sin(\omega t) \tag{5}$$

where X is the magnitude of the vibration displacement. With (1), the equivalent current source should be

$$i_{eq}(t) = \alpha_e X\omega\cos(\omega t). \tag{6}$$

With the parallel connections of C_p, R_p, C_1, and C_2, at open circuit condition, v_p becomes

$$v_{p,oc}(t) = V_{OC}\sin(\omega t + \theta) \tag{7}$$

where

$$V_{OC} = \frac{\alpha_e X\omega R_p}{\sqrt{1+\omega^2 R_p^2(C_p+2C_{ed})^2}} \tag{8}$$

$$\theta = \tan^{-1}\left[\frac{1}{\omega R_p(C_p+2C_{ed})}\right]. \tag{9}$$

V_{OC} is the open circuit voltage, representing the magnitude of v_p; θ is the phase difference between the maximum $v_{p,oc}$ and the zero crossing point (from positive to negative) of i_{eq}, as shown in Fig. 5. Without shunt circuit connected, the original open circuit voltage of the piezoelectric structure is

$$V_{OC,org} = \frac{\alpha_e X\omega R_p}{\sqrt{1+\omega^2 R_p^2 C_p^2}}. \tag{10}$$

Therefore, (8) implies that the open circuit voltage in SP-SSHI will be slightly reduced from $V_{OC,org}$ under the same excitation.

In addition, to effectively drive the switches, there is a constraint for V_{OC}, which is set by the forward voltage drops of diodes and transistors in the circuit. To figure out the constraint, suppose no switching action is performed before the connection of the circuit. Once it is connected, the first switching action may start after v_p attains, for example, its maximum, i.e., V_{OC}, and then drops to $V_{OC} - V_D - V_{BE}$. At this time, T_1 will conduct only when v_{C1} is larger than the voltage drop produced by $T_{1(ec)}$, D_3, $T_{3(be)}$, C_{rect}, and D_8 in series, and T_3 will conduct only when v_p is larger than the voltage drop produced

by D_5, $T_{3(ce)}$, C_{rect}, and D_8 in series. Both yield the same constraint for V_{OC} as

$$V_{OC} > V_{CE(sat)} + 3V_D + V_{BE} + V_{DC} \tag{11}$$

where $V_{CE(sat)}$ is the collector-emitter saturation voltage of the corresponding transistors.

On the other hand, given a V_{DC} satisfying (11), we can obtain the maximum attainable V_{DC} in energy harvesting from (11), as follows:

$$V_{DC,max} = V_{OC} - V_{CE(sat)} - 3V_D - V_{BE}. \tag{12}$$

B. Switching Phase Lag

From the principle of SSHI [11], the switching actions should be taken at the right instants when v_p attains its extreme values, i.e., V_{max} or V_{min} in Fig. 5. In SP-SSHI, however, to switch at the very instants would be impossible; due to the voltage drops of diodes and transistors in the envelope detectors and comparators, there is a phase lag between the instants of switching action start and the maximum (or minimum) v_p. This phase lag is shown as ψ in Fig. 5 and calculated with the following relation:

$$\psi = \cos^{-1}\left(1 - \frac{V_D + V_{BE}}{V_{OC}}\right). \tag{13}$$

Combining (9) and (13), the phase difference between the instants of maximum v_p and maximum displacement (also $i_{eq} = 0$) can be obtained as

$$\varphi = \psi - \theta. \tag{14}$$

This phase difference φ was regarded as constant in [21]. Nevertheless, given the above relations, φ in fact changes with V_{OC}. Considering the constraint on V_{OC} given in (12), the range of φ can be obtained as

$$-\theta < \varphi < \cos^{-1}\left[\frac{V_{CE(sat)} + 2V_D + V_{DC}}{V_{CE(sat)} + 3V_D + V_{BE} + V_{DC}}\right] - \theta. \tag{15}$$

The lower limit corresponds to infinite V_{OC}; the upper one corresponds to the minimum harvestable V_{OC}.

C. Intermediate Voltages among Four Phases

In the externally powered SSHI, there are only two phases in a half vibration cycle, i.e., natural charging and voltage inversion. The two intermediate voltages can be calculated according to the charging and discharging processes in these two phases. In SP-SSHI, owing to the interactions among different parts in the self-powered switching circuit, more phases are distinguished for better analysis about the circuit behavior. Four working phases were introduced in Section III. As shown in Fig. 6, the four phases are linked by four intermediate voltages from V_1 to V_4.

In the switching on maximum, if $V_1 > V_{ref1}$, where

$$V_{ref1} = V_{CE(sat)} + 2V_D + V_{DC} \tag{16}$$

is the first reference voltage, v_p will experience the first inversion. For the first inversion, i.e., from V_1 to V_2, $C_p + C_1$, L_i, and r form an RLC loop for discharging, with the quality factor of

$$Q_1 = \frac{1}{r}\sqrt{\frac{L_i}{C_p + C_{ed}}}. \tag{17}$$

The relation between V_2 and V_1 can be obtained as

$$V_2 - V_{ref1} = \gamma_1(V_1 - V_{ref1}) \tag{18}$$

where

$$\gamma_1 = \begin{cases} -e^{-\pi/(2Q_1)}, & V_1 > V_{ref1}; \\ 1, & \text{others} \end{cases} \tag{19}$$

is the inversion factor of the corresponding RLC loop, whose quality factor is Q_1.

After the first inversion, if $V_2 < V_{ref2}$, where

$$V_{ref2} = -2V_D - V_{DC} \tag{20}$$

is the second reference voltage, v_p will experience one more inversion. For the second inversion, i.e., from V_2 to V_3, C_p in series with C_{CE}, L_i, and r form another RLC loop for discharging, with the quality factor of

$$Q_2 = \frac{1}{r}\sqrt{\frac{L_i(C_p + C_{CE})}{C_p C_{CE}}}. \tag{21}$$

The relation between V_3 and V_2 can be obtained as

$$V_3 - \frac{C_p}{C_{CE}}(V_2 - V_3) - V_{ref2} = \gamma_2(V_2 - V_{ref2}) \tag{22}$$

where

$$\gamma_2 = \begin{cases} -e^{-\pi/(2Q_2)}, & V_2 < V_{ref2}; \\ 1, & \text{others} \end{cases} \tag{23}$$

is the inversion factor of the corresponding RLC loop, whose quality factor is Q_2.

Assuming that the discharge of C_2 starts after the two inversion of v_p, the charge neutralization is regarded as an independent phase. In the charge neutralization, the total charge in C_p, C_1, and C_2 is unchanged. Considering their original voltages, V_4 is related to V_1, V_2, and V_3 with the following equation:

$$(C_p + 2C_{ed})V_4 = C_{ed}(V_1 + V_2) + C_p V_3. \tag{24}$$

After the charge neutralization, the natural charging starts. It lasts for half of a vibration cycle, until v_p reaches $-V_1$, the

start voltage of the switching on minimum. The voltage relation corresponding to this phase can be obtained as follows:

$$-V_1 = V_4 + \frac{1}{C_p + 2C_{ed}} \int_{\frac{\pi/2+\varphi}{\omega}}^{\frac{3\pi/2+\varphi}{\omega}} \left[i_{eq}(t) - \frac{v_p(t)}{R_p} \right] dt. \quad (25)$$

Since the durations of the two inversions and the charge neutralization are much shorter than a half vibration cycle, the v_p waveform can be approximated by splitting the $v_{p,oc}$ one at the switching instants and then moving the adjacent parts against each other to some extent, i.e.,

$$\hat{v}_p(t) = \begin{cases} v_{p,oc}(t) + \frac{V_1 - V_4}{2}, & \left(n - \frac{1}{2}\right)\pi + \varphi < \omega t \\ & \leq \left(n + \frac{1}{2}\right)\pi + \varphi, \\ v_{p,oc}(t) - \frac{V_1 - V_4}{2}, & \left(n + \frac{1}{2}\right)\pi + \varphi < \omega t \\ & \leq \left(n + \frac{3}{2}\right)\pi + \varphi, \end{cases}$$

$$n \in Z. \quad (26)$$

Substituting the approximated v_p in (26) into (25), and given $\omega(C_p + 2C_{ed})R_p \gg 1$, we can have

$$-V_1 = V_4 - 2V_{OC}\cos\varphi + \frac{4V_{OC}\sin\psi + \pi(V_1 - V_4)}{2\omega(C_p + 2C_{ed})R_p}. \quad (27)$$

Equation (27) provides the relations between V_1 and V_4. Combining the linear equations of (18), (22), (24), and (27), the four intermediate voltages from V_1 to V_4 can be solved out, in terms of V_{OC} and V_{DC}.

D. Harvested and Dissipated Powers

The energy flow within the PEH system is of concern for the overall evaluation on the performance of the harvesting systems [20]. Based on the above analyses about the influences of self-powered implementation on the open circuit voltage, switching phase lag, and intermediate voltages, the harvested power as well as the power dissipated during the harvesting process in SP-SSHI can be calculated as follows:

$$P_{h,SP-SSHI} = 2f_0 V_{DC}\left[C_p(V_1 + V_3 - 2V_2) + C_{ed}(V_1 - V_2)\right], \quad (28)$$

$$\begin{aligned} P_{d,SP-SSHI} &= f_0\Big\{(C_p + 2C_{ed})\left[(V_1 - V_{ref1})^2 - (V_4 - V_{ref1})^2\right] \\ &\quad + 2(V_{CE(sat)} + 2V_D)\big[C_p(V_1 + V_3 - 2V_2) \\ &\quad + C_{ed}(V_1 - V_2)\big] \\ &\quad + \frac{1}{\omega R_p}\left[\pi V_{OC}^2 - 4V_{OC}(V_1 - V_4)\sin\psi \right. \\ &\quad \left. + \frac{\pi(V_1 - V_4)^2}{2}\right]\Big\} \end{aligned} \quad (29)$$

where $f_0 = \omega/(2\pi)$ is the vibration frequency in Hz. The three items in (29) estimate the power dissipations produced by the non-ideal voltage inversions, components' voltage drops, and the internal loss within the piezoelectric element. It should be noted that the harvested power here is the net harvested power. The sensing, comparing, and switching units in the circuit in fact are powered by the piezoelectric source. The power consumed in these units has already been included in the total dissipated power given in (29).

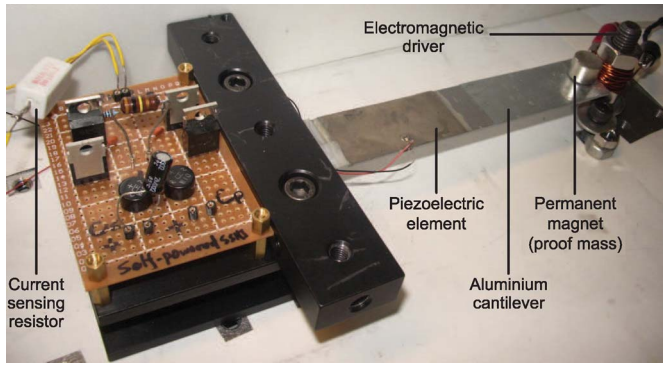

Fig. 8. Experimental setup.

Moreover, the SEH and externally powered SSHI are also employed for the evaluation on the performance of the SP-SSHI. The harvested and dissipated powers in SEH are

$$P_{h,SEH} = 4f_0 C_p V_{DC}(V_{OC,org} - V_{DC} - 2V_D) \quad (30)$$

$$P_{d,SEH} = 8f_0 C_p V_D(V_{OC,org} - V_{DC} - 2V_D). \quad (31)$$

Considering the influence of the internal loss within the piezoelectric element, the expressions on the harvested and dissipated powers in externally powered S-SSHI were provided in [26].[7]

V. Results

Experiments are carried out to evaluate the performance of practical SP-SSHI. The experimental setup is shown in Fig. 8. It is built up with a piezoelectric cantilever and the modified SP-SSHI interface circuit.

The main mechanical structure is an aluminum cantilever whose fixed end is fixed on the vibration-free table while the free end is driven by an electromagnetic driver. A piezoceramic patch of 49 mm × 24 mm × 0.508 mm (T120-A4E-602, Piezo System, Inc.) is bonded near the fixed end where the largest strain happens along the cantilever. A permanent magnet is attached at the free end of the cantilever, so as to achieve the coupling with the electromagnetic driver, and it also acts as a proof mass to lower the vibration frequency and increase the displacement of the free end. A function generator (33120A, Agilent Co.), following by a power amplifier (2706, B & K Co.), provides a 30 Hz sinusoidal excitation to the electromagnetic coil. To provide constant displacement excitation, an inductive displacement sensor (JCW-24SR, CNHF Co.), which is not shown in Fig. 8, is used to measure the displacement

[7] In the externally powered SSHI, the sensing and switching control units do not affect V_{OC}, and there is no switching phase delay; however, the voltage drop of bridge rectifier was considered nonzero in [26].

TABLE II
OTHER CIRCUIT PARAMETERS

Parameter	Value
Diode forward voltage drop V_D	0.5 V
Transistor base-emitter on voltage V_{BE}	0.5 V
Transistor collector-emitter saturation voltage $V_{CE(sat)}$	1.2 V [27]
Transistor emitter-collector capacitance C_{CE}	150 pF [27]
Voltage inversion factor γ_1	-0.78

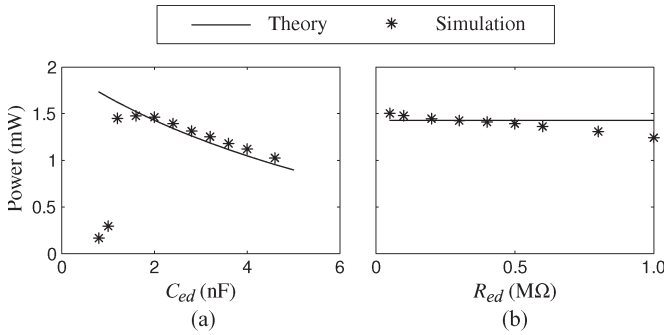

Fig. 9. Sensitivities of the harvested power. (a) Over the capacitance in the envelop detectors, i.e., C_{ed} ($R_{ed} = 200$ kΩ, $V_{OC,org} = 25$ V, $V_{DC} = 10$ V). (b) over the resistance in the envelop detectors, i.e., R_{ed} ($C_{ed} = 2$ nF, $V_{OC,org} = 25$ V, $V_{DC} = 10$ V).

of the cantilever for adjustment under different situations. The circuit component models and values in the experiment are listed in Table I. Other circuit parameters are given in Table II.

As for the selection of components in the self-powered switching interface circuit, the models of the diodes and transistors are not specific; other than these two components, the values of the resistors and capacitors in the envelop detectors, i.e., C_{ed} and R_{ed}, need to be determined according to the inequality given in (4). Fig. 9 shows the sensitivities of the harvested power over the variations of C_{ed} and R_{ed}, respectively. The simulation results for the C_{ed} case match the theory well, except when the C_{ed} is too small to provide enough current for driving the transistors. The effect of R_{ed} is not involved in the theoretical estimation. However, given C_{ed} is fixed at 2 nF, based on the relation provided in (4), the range of R_{ed} is obtained from 125 kΩ to 493 kΩ. The simulation results shown in Fig. 9(b) agree with the theory within this range. Below the lower bound, improper switching actions are observed at local maxima or minima; above the upper bound, the larger R_{ed}, the larger the discrepancy on estimation. In general, with the premise that the SP-SSHI circuit can properly function, the values of C_{ed} should be selected as small as possible, so that the influence caused by the envelop detectors can be minimized; at the same time, the value of R_{ed} should be determined based on (4).

The harvested and dissipated powers under four different excitation levels are investigated. Without the self-powered circuit connected, the four excitation levels induce 5, 8, 12, and 25 volt open circuit voltages $V_{OC,org}$ across the piezoelectric element, respectively. Under those four excitation levels, the harvested power is measured as a function of the storage voltage V_{DC}. Resistors with different resistance values are connected as loads one by one. With the corresponding measured dc voltage across each resistor, the harvested power under different V_{DC} can be obtained. The experimental results of $P_{h,SP-SSHI}$, $P_{d,SP-SSHI}$, and $P_{h,SEH}$ under the four excitation levels, together with the analytical results on the harvested and dissipated powers in the three interface circuits of SP-SSHI, SEH, and ideal SSHI, are shown in Fig. 10 for comparison. From the four subfigures in Fig. 10, both of the analytical and experimental results show good agreement with each other.

Comparing SP-SSHI to ideal SSHI, the higher the excitation level, the closer between the corresponding curves, i.e., $P_{h,SP-SSHI}$ versus $P_{h,SSHI}$ and $P_{d,SP-SSHI}$ versus $P_{d,SSHI}$, which means that the SP-SSHI approaches the ideal SSHI, in terms of both harvested and dissipated powers. Since the total electrical extracted power is composed of harvested and dissipated portions [20], the harvested percentages within the extracted power under different conditions are shown in Fig. 11, where $\tilde{V}_{DC}$ is the nondimensional storage voltage normalized to $V_{OC,org}$. From these figures, the maximum harvested percentage in the SP-SSHI gets higher as the excitation level increases. In addition, under the same excitation level, the harvested percentage in the SP-SSHI might be higher than that in the ideal SSHI case when $\tilde{V}_{DC}$ is small, but in terms of the maximum value, the harvested percentage in the SP-SSHI is less than that in the ideal SSHI.

Comparing the SP-SSHI to SEH, the largest increase in the maximum harvested power is about 200%, as observed from Fig. 10(d). However, meanwhile it should be noted that, unlike the ideal SSHI, whose harvested power has a constant magnification toward that in SEH, the superiority of SP-SSHI over SEH varies. The improvement is more significant under high excitation level; under low excitation, it may lose its benefit. For example, as shown in Fig. 10(a), when $V_{OC,org} = 5$ V, the maximum harvested power in the SP-SSHI is smaller than that in the SEH. On the other hand, for the SP-SSHI under this excitation, the experimental result is even smaller than the theoretical prediction. This is because the transistor in the real circuit cannot be fully turned on and off in time under this low level excitation. Fig. 12 shows the theoretical maximum harvested power as functions of the original open circuit voltage in the SP-SSHI and SEH, respectively. The critical open circuit voltage is 5.84 V for the experimental setup used in this paper. Only when the excitation level is above this critical point, the SP-SSHI can harvest more power than the SEH. On the other hand, as observed from Fig. 11, the harvested percentage in the SEH is always larger than those in the SP-SSHI and the ideal SSHI regardless of the excitation level $V_{OC,org}$ and the storage voltage V_{DC}. In general, rather than claiming that the SP-SSHI always outperforms the SEH, it should be careful to examine the broader range of operation when implementing this SP-SSHI interface circuit.

VI. CONCLUSION

The introduction of the self-powered version of the SSHI did open a promising treatment for PEH with switching technique. Nevertheless, issues still lie in further improvements on both circuit and accurate modeling. We proposed a modified circuit for the SP-SSHI. Compared to the circuitry proposed in [21], the modified circuit not only minimizes the interference

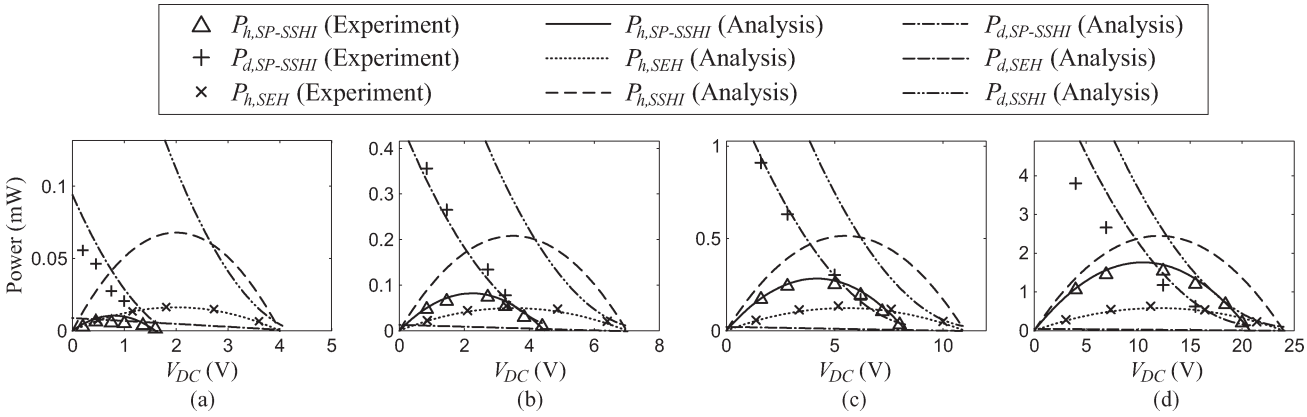

Fig. 10. Harvested and dissipated powers under different excitation levels. (a) $V_{OC,org} = 5.0$ V. (b) 8.0 V. (c) 12.0 V. (d) 25.0 V.

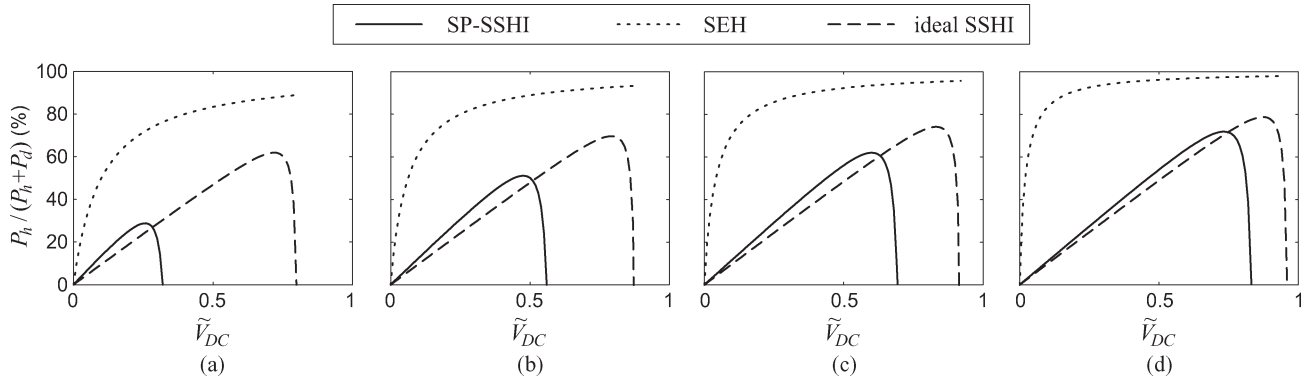

Fig. 11. Harvested percentage within the extracted power. (a) $V_{OC,org} = 5.0$ V. (b) 8.0 V. (c) 12.0 V. (d) 25.0 V.

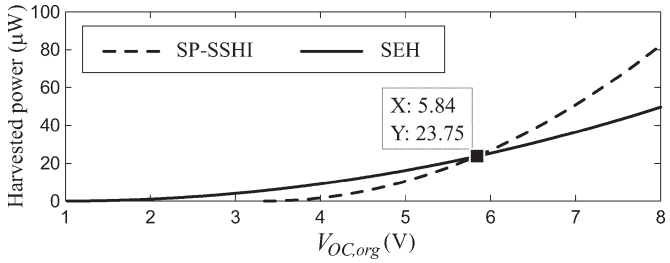

Fig. 12. Maximum harvested power in SP-SSHI and SEH under different excitation levels.

among different units in the circuit, so as can enhance the switching performance, but also results in the removal of some resistive components, so as to further diminish the energy dissipation within the switching processes. Improved analysis was performed considering three aspects, including the open circuit voltage, switching phase lag, and intermediate voltages among different phases. The internal loss with the piezoelectric element was also taken into consideration. Unlike the ideal SSHI, which always has better harvesting capability than SEH, it was found from both analyses and experiments that, for the SP-SSHI, only when the excitation level is high enough, it can outperform the SEH, in terms of the harvested power. Moreover, the higher the excitation level, the more significant the enhancement on harvested power; therefore, the more beneficial to replace the standard interface with such a self-powered switch interface for PEH systems.

REFERENCES

[1] W. H. Liao, D. H. Wang, and S. L. Huang, "Wireless monitoring of cable tension of cable-stayed bridges using PVDF piezoelectric films," *J. Intell. Mater. Syst. Struct.*, vol. 12, no. 5, pp. 331–339, May 2001.

[2] A. Ephremides, "Energy concerns in wireless networks," *IEEE Wireless Commun.*, vol. 9, no. 4, pp. 48–59, Aug. 2002.

[3] J. A. Paradiso and T. Starner, "Energy scavenging for mobile and wireless electronics," *IEEE Pervasive Comput.*, vol. 4, no. 1, pp. 18–27, Jan.–Mar. 2005.

[4] S. R. Anton and H. A. Sodano, "A review of power harvesting using piezoelectric materials (2003–2006)," *Smart Mater. Struct.*, vol. 16, no. 3, pp. R1–R21, Jun. 2007.

[5] A. Khaligh, P. Zeng, and C. Zheng, "Kinetic energy harvesting using piezoelectric and electromagnetic technologies—State of the art," *IEEE Trans. Ind. Electron.*, vol. 57, no. 3, pp. 850–860, Mar. 2010.

[6] Y. K. Tan and S. Panda, "Optimized wind energy harvesting system using resistance emulator and active rectifier for wireless sensor nodes," *IEEE Trans. Power Electron.*, vol. 26, no. 1, pp. 38–50, Jan. 2011.

[7] W. Li, S. He, and S. Yu, "Improving power density of a cantilever piezoelectric power harvester through a curved L-shaped proof mass," *IEEE Trans. Ind. Electron.*, vol. 57, no. 3, pp. 868–876, Mar. 2010.

[8] G. K. Ottman, H. F. Hofmann, A. C. Bhatt, and G. A. Lesieutre, "Adaptive piezoelectric energy harvesting circuit for wireless remote power supply," *IEEE Trans. Power Electron.*, vol. 17, no. 5, pp. 669–676, Sep. 2002.

[9] G. K. Ottman, H. F. Hofmann, and G. A. Lesieutre, "Optimized piezoelectric energy harvesting circuit using step-down converter in discontinuous conduction mode," *IEEE Trans. Power Electron.*, vol. 18, no. 2, pp. 696–703, Mar. 2003.

[10] J. Rocha, L. Goncalves, P. Rocha, M. Silva, and S. Lanceros-Mendez, "Energy harvesting from piezoelectric materials fully integrated in footwear," *IEEE Trans. Ind. Electron.*, vol. 57, no. 3, pp. 813–819, Mar. 2010.

[11] E. Lefeuvre, A. Badel, C. Richard, L. Petit, and D. Guyomar, "A comparison between several vibration-powered piezoelectric generators for standalone systems," *Sens. Actuators A*, vol. 126, no. 2, pp. 405–416, Feb. 2006.

[12] A. Tabesh and L. Frechette, "A low-power stand-alone adaptive circuit for harvesting energy from a piezoelectric micropower generator," *IEEE Trans. Ind. Electron.*, vol. 57, no. 3, pp. 840–849, Mar. 2010.
[13] S. Mehraeen, S. Jagannathan, and K. Corzine, "Energy harvesting from vibration with alternate scavenging circuitry and tapered cantilever beam," *IEEE Trans. Ind. Electron.*, vol. 57, no. 3, pp. 820–830, Mar. 2010.
[14] D. Guyomar, A. Badel, E. Lefeuvre, and C. Richard, "Toward energy harvesting using active materials and conversion improvement by nonlinear processing," *IEEE Trans. Ultrason., Ferroelect.,Freq. Control*, vol. 52, no. 4, pp. 584–595, Apr. 2005.
[15] L. Garbuio, M. Lallart, D. Guyomar, C. Richard, and D. Audigier, "Mechanical energy harvester with ultralow threshold rectification based on SSHI nonlinear technique," *IEEE Trans. Ind. Electron.*, vol. 56, no. 4, pp. 1048–1056, Apr. 2009.
[16] J. R. Liang and W. H. Liao, "Piezoelectric energy harvesting and dissipation on structural damping," *J. Intell. Mater. Syst. Struct.*, vol. 20, no. 5, pp. 515–527, Mar. 2009.
[17] Y. C. Shu, I. C. Lien, and W. J. Wu, "An improved analysis of the SSHI interface in piezoelectric energy harvesting," *Smart Mater. Struct.*, vol. 16, no. 6, pp. 2253–2264, Dec. 2007.
[18] I. C. Lien, Y. C. Shu, W. J. Wu, S. M. Shiu, and H. C. Lin, "Revisit of series-SSHI with comparisons to other interfacing circuits in piezoelectric energy harvesting," *Smart Mater. Struct.*, vol. 19, no. 12, p. 125009, Dec. 2010.
[19] K. Makihara, J. Onoda, and T. Miyakawa, "Low energy dissipation electric circuit for energy harvesting," *Smart Mater. Struct.*, vol. 15, no. 5, pp. 1493–1498, Oct. 2006.
[20] J. R. Liang and W. H. Liao, "Energy flow in piezoelectric energy harvesting systems," *Smart Mater. Struct.*, vol. 20, no. 1, p. 015005, Jan. 2011.
[21] M. Lallart and D. Guyomar, "An optimized self-powered switching circuit for non-linear energy harvesting with low voltage output," *Smart Mater. Struct.*, vol. 17, no. 3, p. 035 030, Jun. 2008.
[22] Y. Ramadass and A. Chandrakasan, "An efficient piezoelectric energy harvesting interface circuit using a bias-flip rectifier and shared inductor," *IEEE J. Solid-State Circuits*, vol. 45, no. 1, pp. 189–204, Jan. 2010.
[23] C. Richard, D. Guyomar, and E. Lefeuvre, "Self-powered electronic breaker with automatic switching by detecting maxima or minima of potential difference between its power electrodes," Patent PCT/FR2005/003000, Jul. 6, 2007.
[24] J. Qiu, H. Jiang, H. Ji, and K. Zhu, "Comparison between four piezoelectric energy harvesting circuits," *Front. Mech. Eng. Chin.*, vol. 4, no. 2, pp. 153–159, Jun. 2009.
[25] N. Krihely and S. Ben-Yaakov, "Self-contained resonant rectifier for piezoelectric sources under variable mechanical excitation," *IEEE Trans. Power Electron.*, vol. 26, no. 2, pp. 612–621, Feb. 2011.
[26] J. R. Liang and W. H. Liao, "On the influence of transducer internal loss in piezoelectric energy harvesting with SSHI interface," *J. Intell. Mater. Syst. Struct.*, vol. 22, no. 5, pp. 503–512, Mar. 2011.
[27] "TIP31C, TIP32C Datasheet," ON Semiconductor, Phoenix, AZ, Tech. Rep., Dec. 2008.

Junrui Liang (S'09–M'10) was born in Guangdong, China, in 1982. He received the B.E. and M.E. degrees in instrumentation engineering from Shanghai Jiao Tong University, Shanghai, China, in 2004 and 2007, respectively, and the Ph.D. degree in mechanical and automation engineering from The Chinese University of Hong Kong, Shatin, Hong Kong, in 2010.

He is currently a Postdoctoral Fellow in The Chinese University of Hong Kong. His research interests include piezoelectric devices, energy harvesting, and Class-E power amplifiers.

Dr. Liang is a recipient of two Best Paper Awards in the IEEE International Conference on Information and Automation (2009 and 2010). He also received the Best Student Contributions Award in the 19th International Conference on Adaptive Structures and Technologies (2008).

Wei-Hsin Liao (M'01–SM'07) received the Ph.D. degree from The Pennsylvania State University, University Park, in 1997.

He is a Professor at the Department of Mechanical and Automation Engineering, The Chinese University of Hong Kong, Shatin, Hong Kong. His research interests include smart structures, vibration control, energy harvesting, mechatronics, and medical devices. His research has led to publications of over 130 technical papers in international journals and conference proceedings, three US patents, and four other US patent applications.

Dr. Liao was the Program Chair for the International Symposium on Smart Structures and Microsystems in 2000, as well as the 2005 IEEE International Conference on Information Acquisition. He was also the Conference Chair for the 20th International Conference on Adaptive Structures and Technologies (ICAST 2009). He currently serves as an Associate Editor for *ASME Journal of Vibration and Acoustics*, *Journal of Intelligent Material Systems and Structures*, as well as *Smart Materials and Structures*. He is a recipient of the T. A. Stewart-Dyer/F. H. Trevithick Prize awarded by the Institution of Mechanical Engineers (2006), the Best Paper Award in Structures from the American Society of Mechanical Engineers (2008), the Best Paper Awards in the IEEE International Conference on Information and Automation (2009 and 2010), and the Best Conference Paper Award in the IEEE International Conference on Mechatronics and Automation (2011). He is a Fellow of the American Society of Mechanical Engineers and Institute of Physics.